3. ATOMIZATION MODELS

The atomization model supplies the initial conditions for spray computations, i.e., the drop sizes, velocities, temperatures etc., at the injector nozzle exit. The fundamental mechanisms of atomization have been under extensive experimental and theoretical study for many years, and reviews of liquid atomization mechanisms have been provided by McCarthy and Molloy (1974) and Reitz and Bracco (1986). In spite of the importance of atomization, the mechanisms of breakup are still not well understood. This makes it difficult to provide the necessary drop size, velocity and trajectory data at the nozzle for spray modeling.

One approach, used for example by Dodge and Schwalb (1989), is to use measured spray characteristics to supply drop size information to models. In their study PDPA radial traverse measurements were made of drop size and velocity distributions, liquid volume fluxes and air velocities at various axial stations far enough downstream of a hollow-cone pressure-swirl atomizer that accurate spray measurements could be made, as depicted in Fig. 3.1a. The measured area-weighted drop size distribution data (Figs. 3.1b and 3.1c) was then combined with drop velocity measurements made 2 mm from the nozzle exit to supply the initial conditions for a spray trajectory calculation using the FLUENT code (see Section 7.2).

The computed and measured results were found to agree very well, as shown in Fig. 3.1d which presents particle trajectories and volume flux comparisons at 50 mm from the nozzle. The good agreement indicates that the processes of drop breakup, drop coalescence and evaporation were relatively unimportant between the nozzle exit and downstream measurement locations for the small-capacity low-pressure spray considered by Dodge and Schwalb (1989).

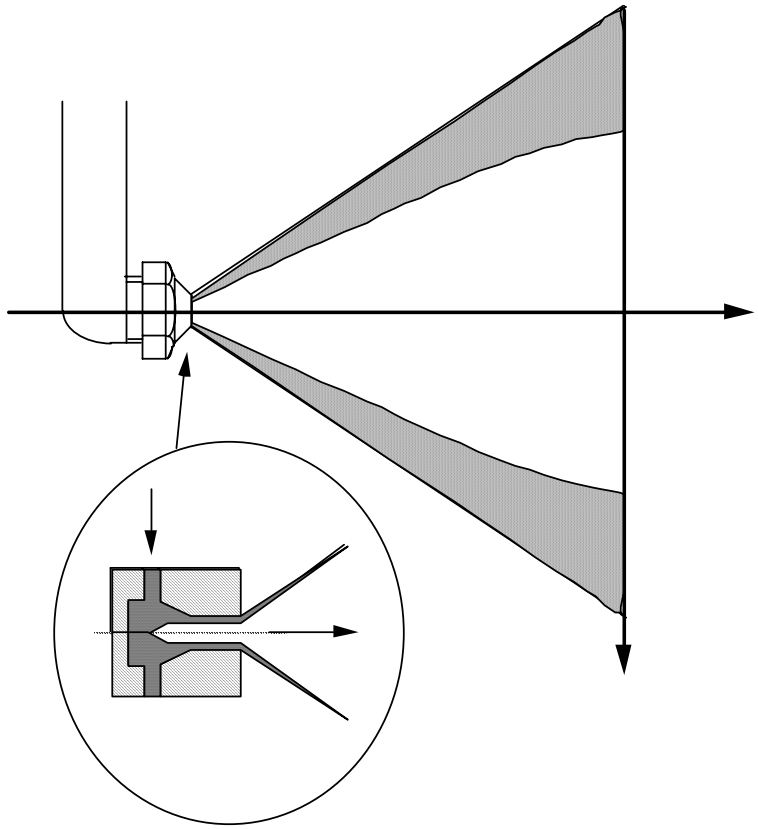

Fig. 3.1a Pressure atomized hollow-cone spray nozzle of Dodge and Schwalb (1989).

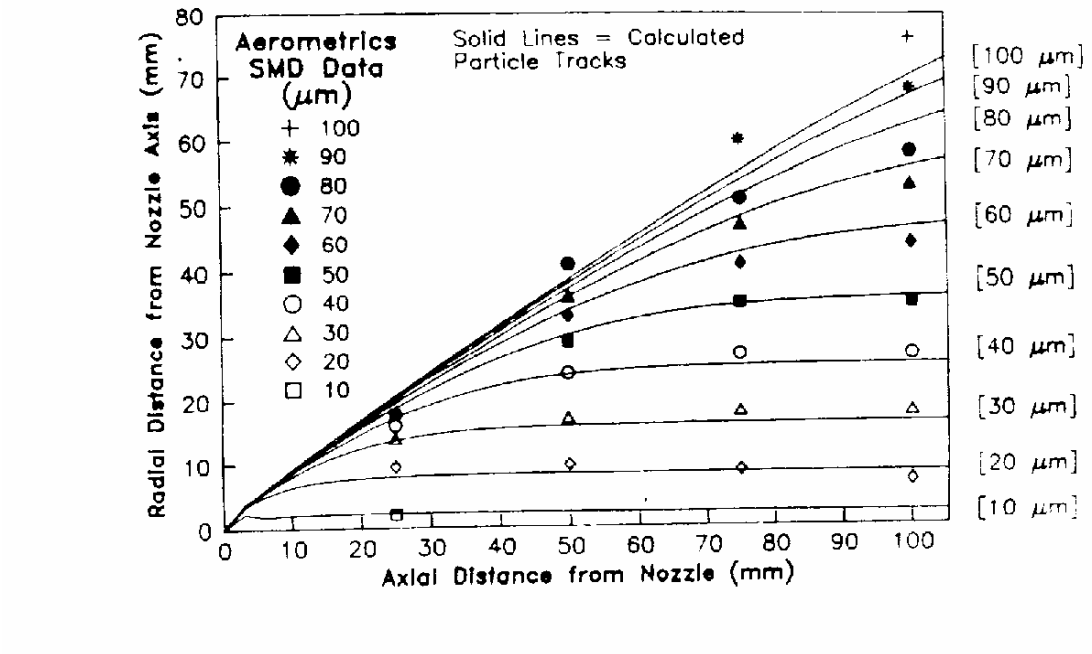

Fig. 3.1b Comparison of drop trajectories measured and predicted by FLUENT of Dodge and Schwalb (1989).

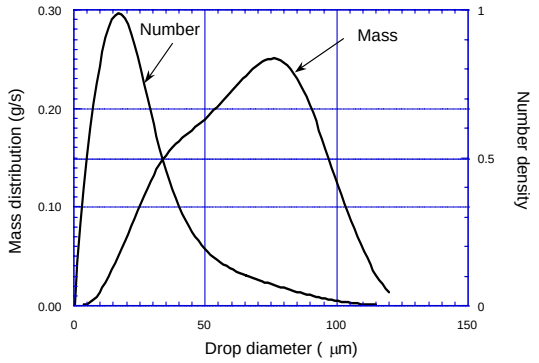

Fig. 3.1c Measured total spray drop size distribution 50 mm downstream of nozzle exit.

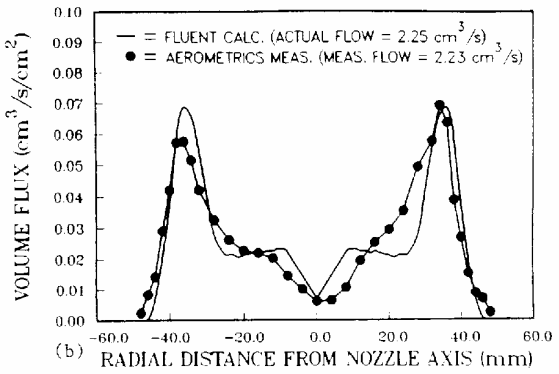

Fig. 3.1d Comparison of measured and predicted volume flux distributions 50 mm downstream of nozzle exit.

However, this procedure of using measured spray data to supply initial conditions for models is not generally possible. Practical difficulties arise in transient spray applications since it is usually not possible to relate downstream drop size measurements to injector exit conditions without a detailed knowledge of the drop velocity, turbulence and air entrainment histories. In other cases the high optical density of the spray drops precludes accurate measurements close to the nozzle and evaporation and breakup/coalescence effects are not negligible within the spray.

Thus, it is necessary to supply initial conditions using models of the atomization process. These models range from linear stability models, as described in Section 3.2, to detailed numerical models based on boundary-element methods (e.g., Hilbing and Heister (1994), Spengler and Heister (1994)) and volume-of-fluid methods (e.g., Mashayek and Ashgriz (1993) and Kothe (1989)).

However, as discussed below, the mechanisms of breakup of liquids are not well understood, even for the relatively simple case depicted in Fig. 2.1 of a constant pressure injection from a single hole nozzle into a stagnant gas. This type of injection gives a conical spray whose divergence starts at the nozzle exit when the gas density is sufficiently high, and there is uncertainty about the inner structure of the spray. Experimental measurements are complicated by the dense spray which is formed since it obscures the breakup details.

Previous studies have established that spray properties are influenced by an unusually large number of parameters, including the conditions in the flow at the nozzle exit, nozzle cavitation effects, the jet velocity and turbulence, and the physical and thermodynamic states of both liquid and gas (e.g., Wu et al., 1992, Eroglu and Chigier, 1991 and Reitz and Bracco, 1979). The precise mechanisms of breakup are still the subject of research (e.g., Chigier and Reitz, 1995).

This Chapter reviews mathematical models that describe the breakup of jets, sheets and drops following the unstable growth of waves on the liquid surface. The wave theory is found to be able to provide qualitative descriptions of breakup phenomena and various breakup regimes. However, the influence of nozzle internal flow effects is only included empirically in the theory, and these effects are known to be important, particularly for high speed breakup. In addition, current breakup models need to be extended to further study the effects of liquid distortion, ligament and membrane formation and stretching on the atomization process. There is also uncertainty about the role of shear stresses (due to viscous effects in the gas) in the liquid breakup process. Most wave breakup models assume that breakup is primarily due to normal stresses at the gas-liquid interface. Additional experiments are needed to be able to resolve the importance of tangential stresses due to the gas viscosity on the liquid breakup process.

The case of a liquid jet injected into a stagnant gas has been most studied in the literature. Jet breakup phenomena have been divided into breakup regimes which reflect differences in the appearance of jets as the operating conditions are changed. The regimes are due to the action of dominant forces on the jet, leading to its breakup, and it is important that these forces be identified in order to explain the breakup mechanism in each regime, as discussed next.

3.1 Jet Breakup Regimes

As shown in Fig. 3.2a, four main breakup regimes have been identified, corresponding to different combinations of liquid inertia, surface tension and aerodynamic forces acting on the jet. These are the Rayleigh, first wind-induced, second wind-induced and the atomization regimes. The growth of small disturbances on the liquid surface due to the interaction between the liquid and ambient gas is believed to initiate the liquid breakup process. The existence of these waves is clearly demonstrated in Figs. 3.2a and 3.2b and, for higher speed jets, in Fig. 3.2c and Fig. 3.2e. The "wave" atomization model to be discussed next attempts to predict the wavelengths and wavegrowth rates of the most unstable surface waves.

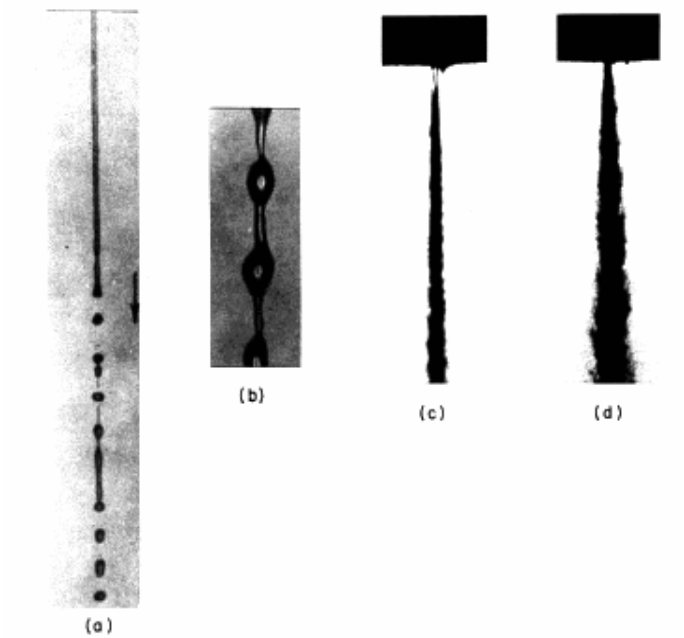

Fig. 3.2 a.) Rayleigh breakup. Drop diameters larger than the jet diameter. Breakup occurs many nozzle diameters downstream of nozzle. b.) First wind-induced regime. Drops with diameters of the order of jet diameter. Breakup occurs many nozzle diameters downstream of nozzle. c.) Second wind-induced regime. Drop sizes smaller than the jet diameter. Breakup starts some distance downstream of nozzle. d.) Atomization regime. Drop sizes much smaller than the jet diameter. Breakup starts at nozzle exit.

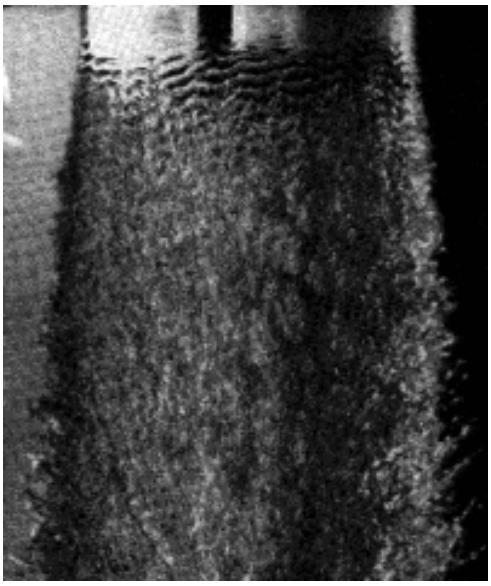

Fig. 3.2e High speed photograph of water jet close to the nozzle exit (at top) in the second wind-induced breakup regime showing surface wave instabilities and breakup (Taylor and Hoyt, 1983).

3.2 "Wave" Breakup Models

The analysis presented here considers the growth of initial perturbations of the liquid surface and includes the effects of liquid inertia, surface tension, viscous and aerodynamic forces on liquid jets and sheets. The theory is found to offer a reasonably complete description of the breakup mechanisms of low speed liquid jets. For high speed jets and sheets however, the initial state of the jet at the nozzle exit appears to be progressively more important and less understood (Reitz and Bracco, 1986, Chigier and Reitz, 1995).

3.2.1 Jet Breakup

The jet breakup theory considers a cylindrical liquid jet issuing from a circular orifice into a stationary, incompressible gas. The stability of the liquid surface to linear perturbations is examined and ultimately leads to a dispersion equation, Eq. (3.3) below, which relates the growth rate, ω, of an initial perturbation of infinitesimal amplitude, to its wavelength λ (or wavenumber $k=2\pi/\lambda$). The relationship also includes the physical and dynamical parameters of the liquid jet and the surrounding gas (Reitz and Bracco, 1982).

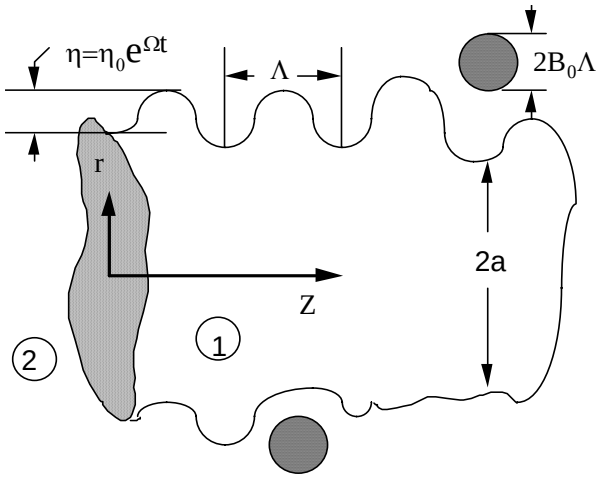

Fig. 3.3 Schematic diagram showing surface waves and breakup on a liquid jet or "blob".

As depicted in Fig. 3.3, the column of liquid is assumed to be infinite in the axial (z) direction and a cylindrical polar coordinate system is used which moves with the liquid-gas relative velocity, U=**v**-**u**. The analysis starts by imposing on the surface an infinitesimal axisymmetric displacement. The equation of the liquid surface is r = a+η, with (see Fig. 3.3)

$$\eta = \mathrm{R}\left(\eta_0 e^{ikz+\omega t}\right) \tag{3.1}$$

where η_0 is the initial amplitude of the disturbance and 'a' is the undisturbed jet radius. Associated with the disturbance is a small axisymmetric fluctuating pressure, p, axial velocity, u, and radial velocity, v, for both the liquid and gas phases denoted by i=1 and 2, respectively. These fluctuations are described by the continuity equation

$$\frac{\partial u_i}{\partial z} + \frac{1}{r}\frac{\partial}{\partial r}(r v_i) = 0$$

and the linearized equations of motion for the liquid and the gas,

$$\frac{\partial u_i}{\partial t} + U_i(r)\frac{\partial u_i}{\partial z} + v_i\frac{dU_i}{dr} = -\frac{1}{\rho_i}\frac{\partial p_i}{\partial z} + \frac{\mu_i}{\rho_i}\left[\frac{\partial^2 u_i}{\partial z^2} + \frac{1}{r}\frac{\partial}{\partial r}\left(r\frac{\partial u_i}{\partial r}\right)\right]$$

$$\frac{\partial v_i}{\partial t} + U_i(r)\frac{\partial v_i}{\partial z} = -\frac{1}{\rho_i}\frac{\partial p_i}{\partial r} + \frac{\mu_i}{\rho_i}\left[\frac{\partial^2 v_i}{\partial z^2} + \frac{\partial}{\partial r}\left(\frac{1}{r}\frac{\partial r v_i}{\partial r}\right)\right]$$

subject to boundary conditions at the interface that include the kinematic jump condition, Eq. (2.4), the normal stress balance, Eq. (2.5), and the tangential stress balance, Eq. (2.6). The normal stress balance accounts for surface tension, dynamic pressure (inertia), viscous (normal) force and recoil forces (due to vapor leaving the interface of an evaporating jet). In the tangential stress balance the gas is typically assumed to be inviscid, i.e., slip is presumed at the liquid-gas interface. This assumption thus does not allow for the presence of shear in the boundary layer in the gas flow at the interface.

The liquid hydrodynamical equations are solved with solutions $\phi_1 = C_1 I_0(kr) \exp(ikz+\omega t)$ and $\psi_1 = C_2 r I_1(lr) \exp(ikz+\omega t)$. ψ_1 and ϕ_1 are the stream function and velocity potential, C_1 and C_2 are integration constants, $l^2=k^2+\omega/\nu_1$, ν_1 is the liquid kinematic viscosity and I_0 and I_1 are modified Bessel functions of the first kind. The liquid pressure is found from $p_1 = -\rho_1 \partial\phi_1 / \partial t$ where ρ_1 is the liquid density.

With the assumption that $\eta << a$, the gas equations of motion yield for the gas pressure at the interface r=a

$$p_2 = -\rho_2 (U - i\frac{\omega}{k})^2 k\eta \frac{K_0(ka)}{K_1(ka)}$$

when it is assumed that the gas is inviscid (K_0 and K_1 are modified Bessel functions of the second kind) and U is the relative velocity between the jet and the gas. The kinematic, tangential and normal stress equations at the interface reduce to

$$v_1 = \mathbf{w} = \frac{\partial\eta}{\partial t}, \qquad \frac{\partial u_1}{\partial r} = -\frac{\partial v_1}{\partial z} \tag{3.2a}$$

$$-p_1 + 2\nu_1\rho_1 \frac{\partial v_1}{\partial r} - \frac{\sigma}{a^2}(\eta + a^2 \frac{\partial^2\eta}{\partial z^2}) + p_2 = 0 \tag{3.2b}$$

(u_1, v_1 are the axial and radial liquid velocity components). Equations (3.2a) are used to eliminate C_1 and C_2, and when the velocity and pressure solutions are used in Eq. (3.2b), this leads to the dispersion relation (Reitz and Bracco, 1982)

$$\omega^2 + 2\nu_1 k^2 \omega \left[\frac{I_1'(ka)}{I_0(ka)} - \frac{2kl}{k^2+l^2}\frac{I_1(ka)}{I_0(ka)}\frac{I_1'(la)}{I_0(la)}\right] = \frac{\sigma k}{\rho_1 a^2}\left(1 - k^2a^2\right)\left(\frac{l^2 - k^2}{l^2 + k^2}\right)\frac{I_1(ka)}{I_0(ka)}$$

$$+\frac{\rho_2}{\rho_1}(U - i\omega/k)^2 k^2 \left(\frac{l^2 - k^2}{l^2 + k^2}\right)\frac{I_1(ka)K_0(ka)}{I_0(ka)K_1(ka)} \qquad (3.3)$$

Solutions of Eq. (3.3) are presented in Fig. 3.4 which shows predicted wave growth rates versus non-dimensional wave length as a function of the jet Weber and Ohnesorge numbers, We_2 and Z. The results indicate that there is a maximum wave growth rate, Ω, that occurs at a wave length of Λ. The maximum wave growth rate and the corresponding wavelength characterize the fastest growing (or most probable) waves on the liquid surface which are thought to be eventually responsible for the breakup.

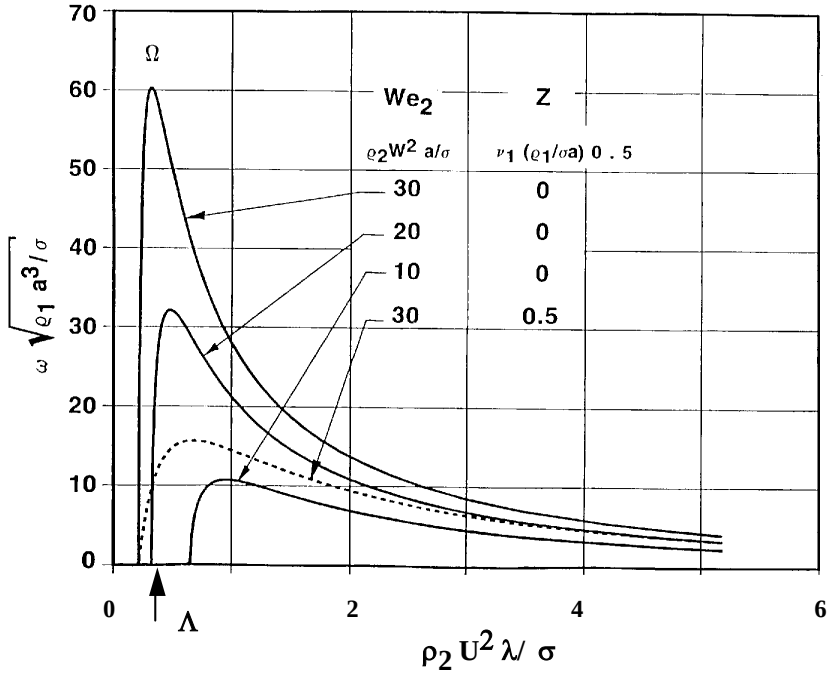

Fig. 3.4 Wave growth rate versus wave number as a function of Weber number and Ohnesorge number. The maximum wave growth rate and length scale are Ω and Λ, respectively.

Reitz (1987) generated curve-fits of numerical solutions to Eq. (3.3) for the maximum growth rate ($\omega=\Omega$) and for the corresponding wavelength ($\lambda=\Lambda$):

$$\frac{\Lambda}{a} = 9.02\,\frac{\left(1+0.45Z^{0.5}\right)\left(1+0.4T^{0.7}\right)}{\left(1+0.87We_2^{1.67}\right)^{0.6}} \tag{3.4a}$$

$$\Omega\left(\frac{\rho_1 a^3}{\sigma}\right)^{0.5} = \frac{0.34+0.38\,We_2^{1.5}}{(1+Z)\left(1+1.4T^{0.6}\right)} \tag{3.4b}$$

$$Z=\frac{We_1^{0.5}}{Re_1};\quad T=ZWe_2^{0.5};\quad We_1=\frac{\rho_1 U^2 a}{\sigma};\quad We_2=\frac{\rho_2 U^2 a}{\sigma};\quad Re_1=\frac{Ua}{\nu_1}$$

Equations (3.4a) and (3.4b) are shown in Figs. 3.5a, b. As can be seen, the maximum wave growth rate increases and the corresponding wavelength decreases rapidly with increasing Weber number. The effect of viscosity which appears in the Ohnesorge number, Z, is seen to reduce the wave growth rate and increase the wave length significantly as the liquid viscosity increases.

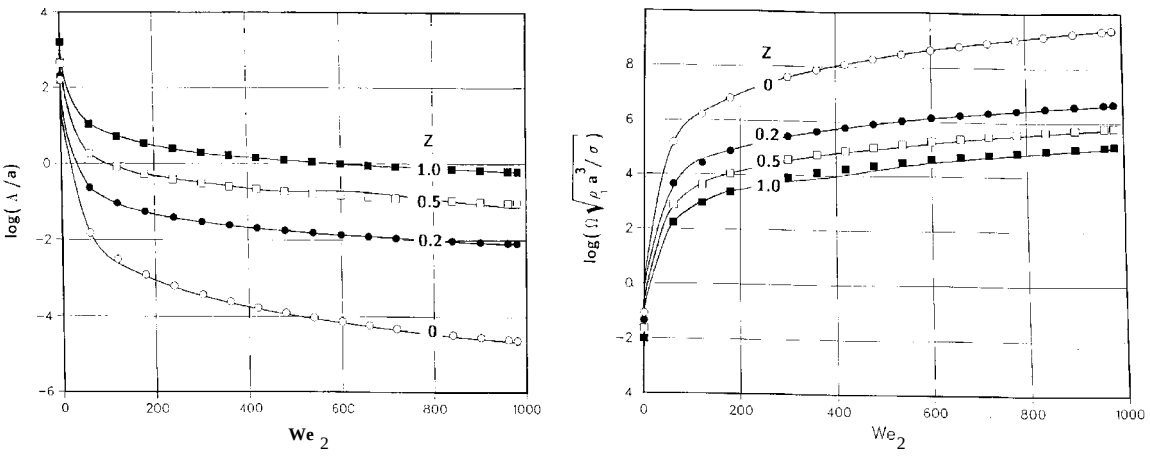

a.) b.)

Fig. 3.5 Wavelength a.) and growth rate b.) of the most unstable surface wave versus Weber number, We_2, as a function of Ohnesorge number, Z (Reitz, 1987).

Equation 3.3 has also been used as a framework to organize jet breakup regimes (Reitz, 1987). At low Weber numbers, We_2, breakup is in the Rayleigh regime (Fig. 3.2a), and the drop sizes are larger than the jet diameter. In this case, in the normal stress equation. Eq. (3.2b) there is a balance between the inertia (i.e., the liquid dynamic pressure) and surface tension terms. The jet surface is unstable for all wavenumbers with $ka < 1$ and the maximum growth rate occurs at $\Lambda=9.02a$ (see Eq. (3.4) with $We_2=0$ and $T=0$). Inclusion of the viscous normal stress involves the liquid viscosity through the Ohnesorge number, Z. This moves the most unstable wave to longer wavelengths, but the jet breakup agency remains the destabilizing combination of surface tension and inertia forces. The liquid viscosity term has a secondary stabilizing effect also in the other breakup regimes.

The inertial effect of the surrounding gas enters as the Weber number We_2 is increased. As seen in Eq. (3.4b), this enhances the wave growth rate, but the drop sizes are still of the order of the jet diameter in the first wind-induced breakup regime (Fig. 3.2b). With further increases in We_2, the gas inertia effect increases. The maximum growth rate occurs at progressively shorter wavelengths and, eventually, the breakup is due to unstable growth of short wavelength surface waves. Drops are formed with sizes much less than the jet diameter (Fig. 3.2c and Fig. 3.2e). Equations (3.4a) and (3.4b) become independent of the jet diameter when We_2 is sufficiently large. Reitz and Bracco (1986) call this the second wind-induced breakup regime.

The final regime, the atomization regime (Fig. 3.2d), is reached in the high Weber number limit when the gas density is sufficiently high. This is the regime of interest in high-pressure sprays such as in diesel engines where breakup commences at (or very near) the nozzle exit. Previous studies suggest that the surface wave mechanism of the second wind induced regime could still apply to jets in the atomization regime (Reitz and Bracco, 1982). However, direct verification of this mechanism by means of experiment has not yet been possible because the dense spray which surrounds the jet obscures the breakup details.

Extensions of the wave stability analysis have been performed by various authors. For example, Ibrahim (1993) has considered the effect of liquid swirl which was found to enhance jet atomization. The most unstable wave growth rate increases and the wavelength decreases with increased liquid swirl. Lian and Lin (1990) considered the effect of gas swirl which was found to hinder atomization. The cases of evaporating jets and compressible gas flows have

been considered by Lian and Reitz (1993). Vaporization destabilizes low speed jets and stabilizes high speed jets. The effect of gas compressibility was found to destabilize subsonic jets. Experiments have been conducted on supersonic jets by Issac et al. (1994) which indicate that the unstable growth of surface waves is responsible for the breakup in the high velocity jet breakup case too. The breakup of a liquid jet injected into an immiscible liquid has also been studied by various authors. In this case it is not justifiable to neglect the continuous phase viscosity in the tangential and normal stress balances at the interface. A recent review is given by Richards et al. (1994).

The results of jet stability analyses have been used to estimate the sizes of drops formed during the atomization process by assuming that the drop size is linearly related to the wavelength, Λ (e.g., Taylor, 1940) (see Fig. 3.3). For inviscid liquid jets at high gas Weber numbers, Reitz and Bracco (1979) give for the drop radius, r

$$r = B2\,\pi\frac{\sigma}{\rho_g U^2} \qquad (3.5)$$

where B is a constant of order unity, and ρ_g is the gas density. Equation (3.5) follows from Eq. (3.4a) for Z=0 and large We_2. Wu et al. (1986) compared the predictions of Eq. (3.5) with measured drop sizes at the edge of a diesel-type spray near the nozzle exit, and concluded that the model gave reasonable results provided that drop collision and coalescence effects were accounted for in the dense spray between the atomizing surface and the edge of the spray.

Experiments on diesel-type sprays show that there is an "intact" core region of unbroken liquid within the spray near the nozzle exit, however, the precise length of the core is still the subject of research. To account for the fact that atomization does not occur immediately at the nozzle exit, Chatwani and Bracco (1985) injected drops with sizes obtained from Eq. (3.5) using the 'line-source' model shown in Fig. 3.6. Here it is assumed that the drops are formed along a line that is aligned with the spray axis and is much longer than the nozzle radius. The length of the core is found from considerations of the mass removed from the jet by the atomization process, and is given by (Taylor, 1940)

$$L = C\,a\sqrt{\frac{\rho_1}{\rho_2}} \,/\, \mathrm{f}(T) \qquad (3.6)$$

where a is the nozzle radius, and the function f(T) is shown in Fig. 3.7a and asymptotically equal to $3^{1/2}/6$ for T>100 (typical diesel sprays have T>>100). The constant C has been found to be in the range 14-30 (Cheroudi et al., 1985).

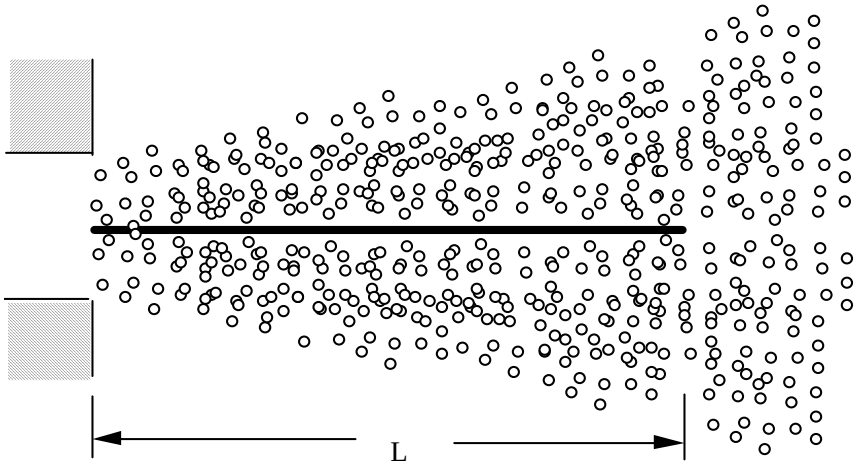

Fig. 3.6 Line-source atomization model (Chatwani and Bracco, 1985).

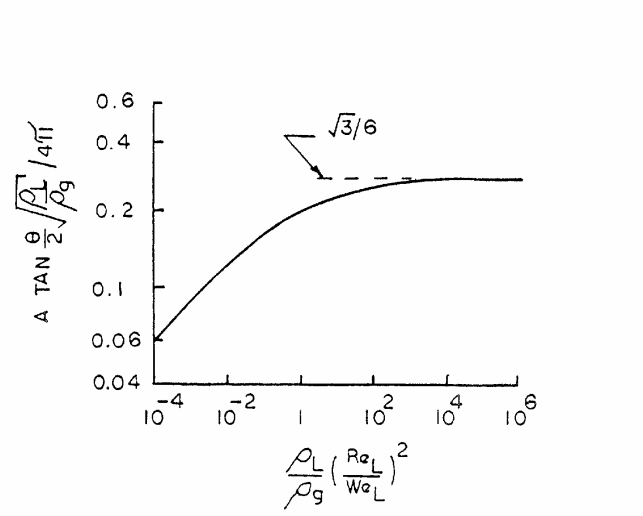

Fig. 3.7a Theoretical dependence of the spray angle parameter f(T) on Taylor's number $T=\rho_L/\rho_g\ (Re_L/We_L)^2$ (subscripts L and g refer to the liquid and gas phases, respectively).

To account for the spreading of the spray near the nozzle exit, the drops are typically injected with a velocity component normal to the spray axis in computational models, as depicted in Fig. 3.7b. By assuming that the ejected drop's velocity, v, is proportional to the wave growth rate, Reitz and Bracco (1979) give

$$Tan\theta = \frac{v}{U} = \frac{1}{A} 4\pi \left(\frac{\rho_g}{\rho_l}\right)^{1/2} f(T) \qquad (3.7)$$

where, for sharp-edge inlet nozzles, the constant, A, is related to the nozzle passage length-to-diameter ratio, l/d, as A=3.0+(l/d)/3.6.

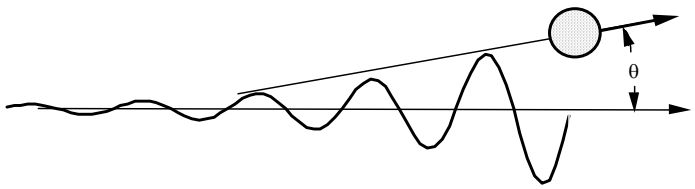

Fig. 3.7b The spray angle, θ, is determined from the wave growth rate by injecting drops with a normal velocity component, v.

3.2.2 Sheet Breakup

Linear stability analyses have also been conducted for describing the breakup of liquid sheets. The capillary instability of thin liquid sheets was first studied by Squire (1953) who showed that instability and breakup are caused by the growth of sinuous waves (sideways deflections of the sheet centerline), as depicted in Fig. 3.8a. Figure 3.8b shows experimental results for the controlled breakup of a fan-spray that was perturbed with an externally supplied oscillation (Van Dyke, 1978). The formation of orderly rows of ligaments from the breakup of the sheet is clearly seen, together with large drops that originate from the rims of the sheet.

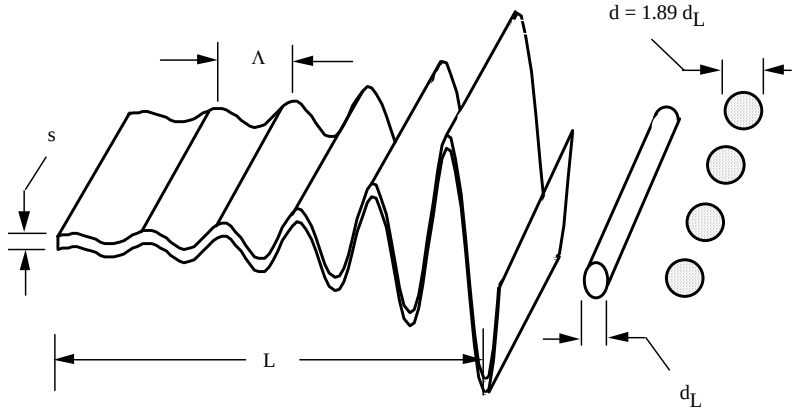

Fig. 3.8a Breakup mechanism of liquid sheets.

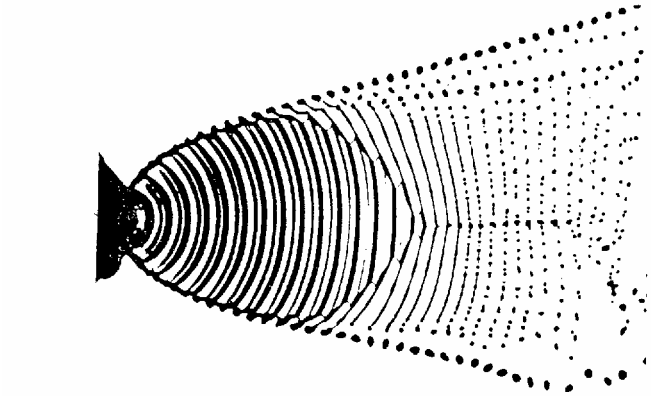

Fig. 3.8b Induced breakup of a liquid sheet from a perturbed fan-spray nozzle (Van Dyke, 1982).

Meyer and Weihs (1987) conducted an analysis of an annular liquid jet, including the limits of the circular liquid jet or a cylindrical cavity in a liquid medium (when the ratio of the internal to external annulus radii tend to zero) and the thin planar sheet (when the radius ratio tends to unity). For inviscid liquids, their results show that, when the annulus thickness is greater than a critical thickness, $t=\sigma/(\rho_g U^2)$, the annular jet behaves like a full liquid jet. When the annulus thickness is less than the critical thickness, the jet behaves like a two-dimensional liquid sheet. For low viscosity liquid sheets, Fraser et al. (1963) give the wavelength of the dominant unstable wave as $\Lambda=4\pi\sigma/(\rho_g U^2)$, where U is the root-mean-square of the relative liquid-gas velocities on the two sides of the sheet. A similar result has been derived by Li (1994) who considers both the sinuous and varicose instability modes. Photographs of sheet breakup show that the thin sheet rapidly contracts into a ligament (see Fig. 3.8) at the breakup point. The ligament diameter, d_L, can be estimated by assuming that it contains all of the liquid in one-half of a wavelength from $d_L=(4\Lambda s/\pi)^{1/2}$, where s is the sheet thickness (Fraser et al., 1963). Since a liquid column is an unstable configuration, the ligament then breaks up under the action of surface tension forces, as seen in Fig. 3.8b. From Rayleigh's analysis of the breakup of a low speed liquid jet, the breakup of the ligaments produce drops of diameter $d = 1.89\, d_L$, so that the drop radius is (Fraser et al., 1963)

$$r = 2 \cdot 1.89 \sqrt{\frac{\sigma s}{\rho_2 U^2}} \qquad (3.8)$$

The breakup length has been estimated for liquid sheets by Clark and Dombrowski (1972) from Squire's theory who give

$$L = D \sqrt[3]{\frac{\rho_l \sigma K \ln(\eta / \eta_0)}{\rho_g{}^2 U^2}} \qquad (3.9)$$

where the constant D=20 (Reitz and Diwakar, 1986), η is the wave amplitude when the sheet breaks up, and the parameter $\ln(\eta/\eta_0)$ is

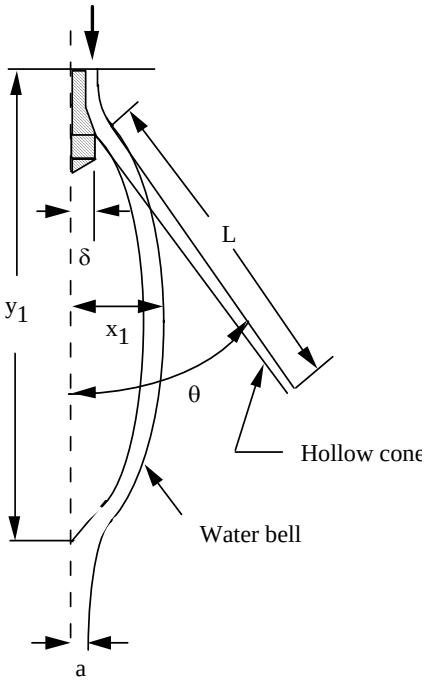

Fig. 3.9a Poppet nozzle sheet breakup schematic diagram

determined experimentally to be equal to 12. For an attenuating sheet, the sheet thickness is inversely proportional to its distance from the origin and K = 2sx, is computed knowing the sheet thickness at some distance, x, from the nozzle. For a "hollow-cone" spray nozzle with cone (half) angle, θ, and poppet seat diameter, δ, and sheet thickness, h, at the nozzle exit, as shown in Fig. 3.9a, Reitz and Diwakar (1986) give for the breakup length

$$L / \delta = D_3 \sqrt{(\frac{\rho_l}{\rho_g})(\frac{\sigma}{\rho_g U^2 \delta})(\frac{h}{\delta})\frac{1}{Tan\theta}} \qquad (3.10)$$

and, hence, from Eq. (3.8) the drop size is

$$r = 8.4 D^{-3/2} L \sqrt{\frac{\rho_g}{\rho_l}} \qquad (3.11)$$

Figures 3.9b and c show photographs of breakup from a Bosch automotive port fuel injector (θ=12.5 degrees, δ=0.84 mm) using water and indolene (σ=70 and 19 g/s^2, ρ_L=1.0 and 0.7 g/cm^3, respectively) in a mild cross-flow (from left to right).

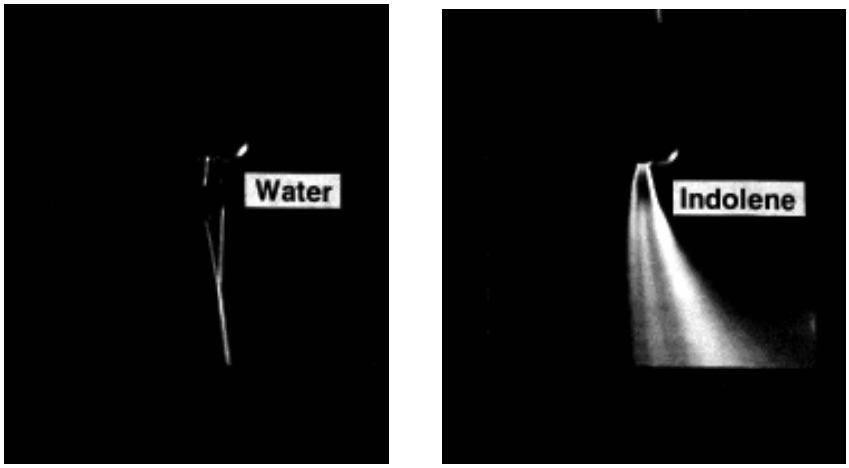

b.) c.)

Fig. 3.9 (cont.) Sheet breakup regimes from poppet-type nozzles.
b.) water bell breakup, c.) indolene hollow-cone sheet breakup.

In Fig. 3.9b the conical liquid sheet emerging from the nozzle annulus closes in on itself forming a bell that is followed by a roughly cylindrical liquid jet. The recombined liquid jet breaks up into a full-cone spray of large drops downstream of the bell. In Fig. 3.9c the liquid sheet disintegrates into a hollow-cone spray of small drops before a bell can be formed.

Criteria for predicting the boundary between the two different regimes can be formulated by using the results of Taylor (1959). The bell reattachment length, y_1, and the width, x_1, (see Fig. 3.9a) are given by

$$y_1 / F(\theta) = x_1 / G(\theta) = \rho_1 U^2 \delta h / 2\sigma \qquad (3.12)$$

where $F(\theta)=2 \ln(\sec\theta+(\sec^2\theta-1)^{1/2})$ and $G(\theta)=1-\cos\theta$.

The ratio of y_1 (from Eq. 3.12) to the sheet breakup length L (from Eq. 3.10) serves as a predictor of the breakup regime. For the conditions of Fig. 3.9b and 3.9c, y_1/L is estimated to be 1.59 and 0.21, respectively. This indicates that $y_1/L=1$ may be a reasonable criterion to use for estimating the location of the regime boundary. Note that for good atomization (i.e., sheet breakup), Eqs. (3.10) and (3.12) indicate that small y_1/L values are required. This is achieved with low surface tension, high gas density, high injection pressure (velocity), and large nozzle cone angles.

3.3 "Blob" Injection Model

Reitz (1987) applied the "wave" stability atomization theory to diesel spray modeling, by injecting parcels of liquid in the form of "blobs" that have a characteristic size equal to the nozzle hole diameter, instead of assuming an intact liquid at the nozzle exit. The basis of this model is the concept introduced by Reitz and Diwakar (1987) that the atomization of the injected liquid and the subsequent breakup of drops are indistinguishable processes within a dense spray. As depicted in Fig. 3.10, a core region is predicted to exist near the nozzle with the "blob" model because, although the injected liquid breaks up due to its interaction with the surrounding gas as it penetrates into the gas, there is a region of large discrete liquid particles near the nozzle, which is conceptually equivalent to a core of churning liquid ligaments within the context of a sub-grid-scale model (c.f. Fig. 2.1).

In the model of Reitz and Diwakar (1987) the liquid was injected as discrete parcels (blobs) which broke up using experimental drop breakup correlations given in Section 4.1 below. In the study of Reitz (1987), the blobs breakup using the results from the jet stability theory. In this case, liquid breakup is modeled by postulating that new drops are formed (with drop radius, r) from a parent drop or blob (with radius, a) with

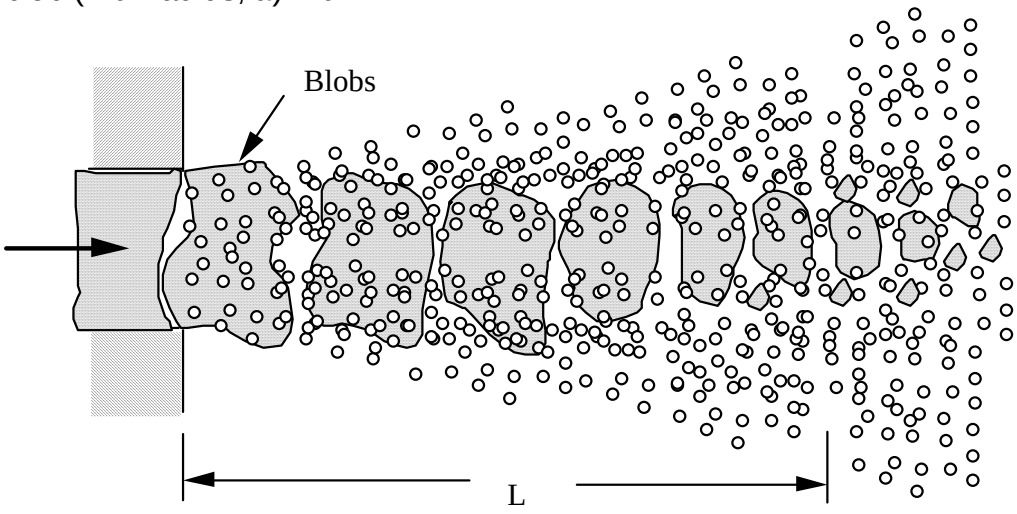

Fig. 3.10 "Blob" injection breakup model (Reitz and Diwakar, 1987)

$$r = \quad B_0\Lambda \qquad (B_0\Lambda \leq a) \qquad (3.13a)$$

$$r = min\begin{cases} (3\pi a^2 U/2\Omega)^{0.33} \\ \\ (3a^2\Lambda/4)^{0.33} \end{cases} \qquad (B_0\Lambda > a, \text{ one time only}) \qquad (3.13b)$$

where $B_0 = 0.61$. In Eq. (3.13a), it is assumed that small drops are formed with drop sizes proportional to the wavelength of the fastest-growing or most probable unstable surface wave; Eq. (3.13b) applies to drops larger than the jet (i.e., for low speed breakup) and assumes that the jet disturbance has frequency $\Omega/2\pi$ (a drop is formed each wave period) or that drop size is determined from the volume of liquid contained under one surface wave.

The mass of new droplets formed due to breakup is subtracted from the parent drops as the breakup proceeds. The change of the radius of a parent drop or "blob" is assumed to follow the rate equation

$$da/dt = -(a - r)/\tau \qquad (r \leq a) \qquad (3.14)$$

where τ is the breakup time,

$$\tau = 3.726 B_1 \, a / \Lambda\Omega \qquad (3.15)$$

B_1 is the breakup time constant with the suggested value B_1=20 (Reitz, 1987). However, this value has been found to depend on the injector characteristics and other values can be found in the literature, e.g., B_1=1.73 by O'Rourke and Amsden (1987), B_1=30 by Patterson et al. (1994).

Figures 3.11a, b, c and d show computational results obtained by applying the "blob" injection technique to sprays from a single hole orifice. The computations were made using the KIVA code and results are shown for jets at 2.4 ms (Figs. 3.11a, b and c) and 12.0 ms (Figs. 3.11d) after the start of injection. The injector is oriented vertically downward in each diagram. The injection velocity was 40 m/s, the nozzle diameter was 0.2 mm (l/d=4) and the liquid and gas temperature was 298 K in each case. The spray liquid was tetradecane (ρ_1=770 g/L, σ=21.8 g/s^2, ν_1=2.5 mm^2/s). The only quantity varied was the air

pressure (density) which was 50, 200, 500 and 2500 kPa for Figs. 3.10a, b, c and d, respectively.

Unbroken injected liquid blobs are shown as solid circles. The even spacing between blobs (which is seen clearly in Fig. 3.11a) reflects the discrete blob injection method. Spray parcels are produced from the breakup of these blobs and the parcel locations are shown as open circles. The size of each circle is proportional to the size of the drops in the parcel (of course, drop size is exaggerated greatly in the figures and the number of spray drops in each parcel is not shown).

In Fig. 3.11a (We_g=9.0), the liquid blobs break up only after a long intact length and the drop sizes are larger than the original jet (blob) diameter, as in the low-speed Rayleigh breakup regime. The jet tip penetration is 97 mm which is close to the product of the injection velocity and the elapsed time (i.e., the jet penetrates like a solid rod). In Fig. 3.11b (We_g=36), the jet breaks up sooner and the resulting drops are smaller than those of Fig. 3.11a, as for a jet in the first wind induced regime. Jet tip penetration is reduced due to increased momentum transfer between the jet and the ambient air.

A short intact (unbroken) region of the jet can still be seen close to the nozzle exit in the spray of Fig. 3.11c (We_g=90). Further downstream drops are produced with sizes much smaller than the nozzle diameter, as for a jet in the second wind induced regime. The jet tip penetration is reduced further due to the increased gas density. Finally, in Fig. 3.11d (We_g=452), there is no longer any evidence of unbroken liquid near the nozzle and the spray drops are smaller than the nozzle diameter, as for a jet in the atomization regime. The spray penetration is reduced considerably.

The above trends are seen to agree very well with the jet breakup features shown in the photographs of Fig. 3.1, giving confidence to the "wave" atomization model predictions. However, the predicted values of the Weber numbers in the various regimes are somewhat higher than those given by available regime criteria (Chigier and Reitz, 1995). This may be due to the fact that those criteria do not account for nozzle flow effects. Similarly, there are uncertainties in the breakup time model constant in Eq. (3.15), which also does not account for nozzle internal flow effects.

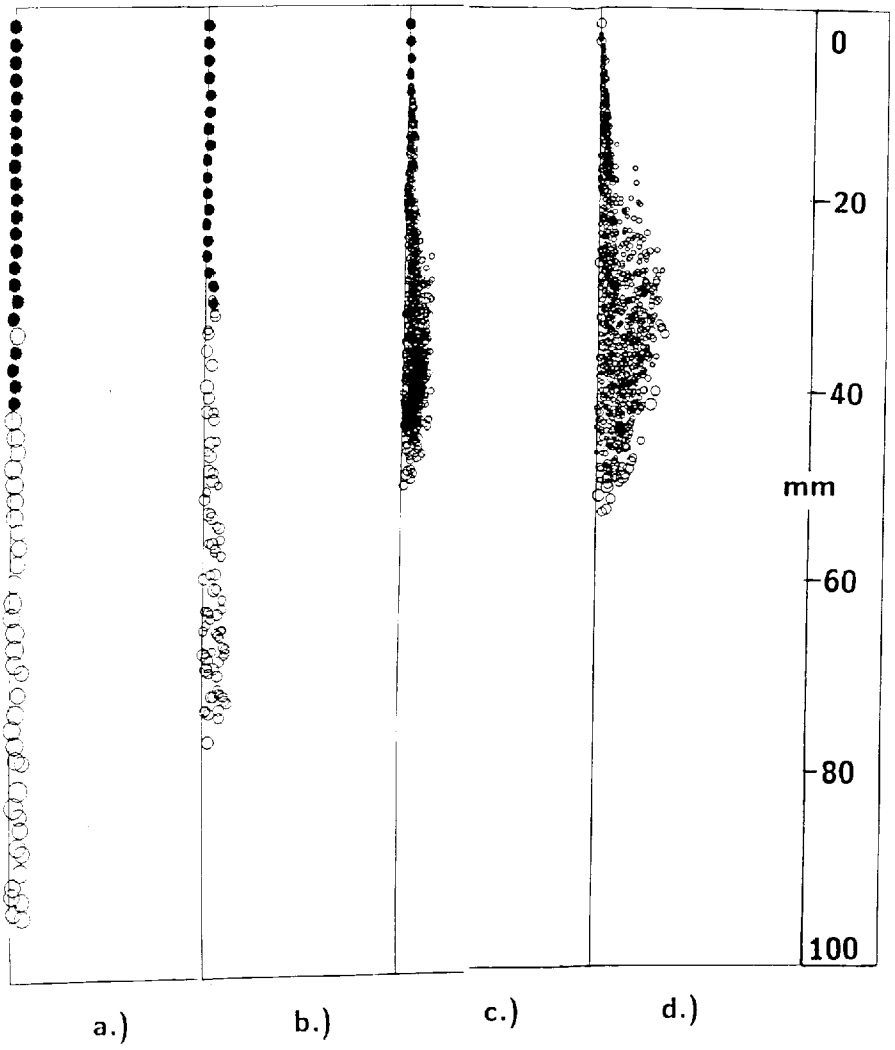

Fig. 3.11 Predictions of jet breakup regimes (Reitz (1987).
a.) We_g=9 b.) We_g=36 c.) We_g=90 d.) We_g=452. a), b) and c) shown at 2.4 ms after the beginning of injection, spray d) at 12 ms. Solid circles - unbroken injected liquid blobs. Open circles - drops (drop size is proportional to size of the circles).

To study the structure of atomizing jets, comparisons were made with measurements of Hiroyasu and Kadota (1974) of spray tip penetration and drop size. The nozzle diameter was 0.3 mm and the computations used tetradecane for the spray liquid (the experiments used a diesel fuel oil with physical properties close to tetradecane) and the liquid and gas temperature was 298 K. Three injection pressures of 1.1, 3.0 and 5.0 MPa were used in the experiments.

Figures 3.12a, b and c show spray parcel locations for the three sprays (2.5 ms after the start of the injection for the 1.1 MPa case and at 4.5 ms for the 3.0 and 5.0 MPa cases). The fact that unbroken liquid is present in the core region is indicated by the plots at the right of each spray which show only those parcels containing drops larger than 180 μm in diameter. These plots show that the core length decreases with increasing gas density, consistent with the correlation presented in Eq. (3.6). The arrows indicate the point

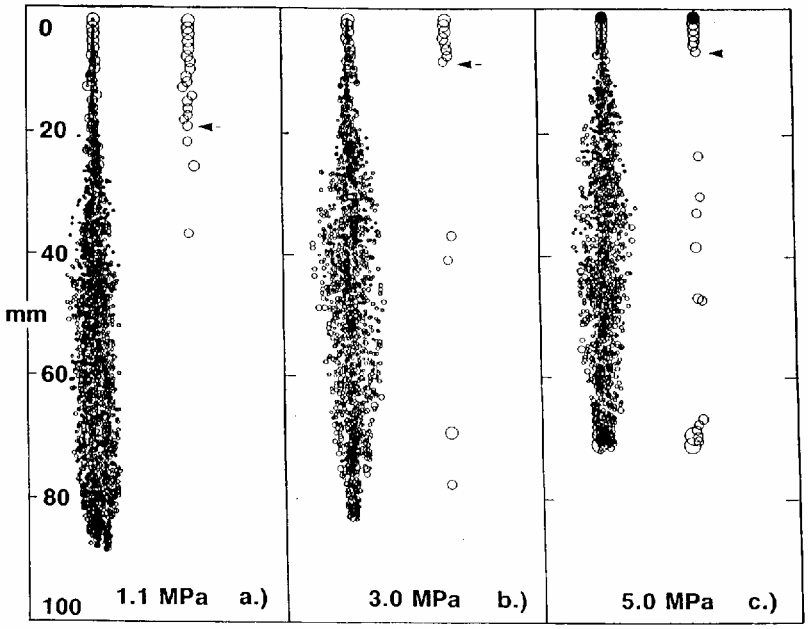

Fig. 3.12 Spray parcel plots showing co-existing large drops and small product drops in the core region near the nozzle. Plots at the right show only the parcels containing drops with diameters larger than 180 μm (Reitz, 1987).

chosen to represent the position of the last 180 μm drops in the core. Some large drops are also seen downstream of the core in Fig. 3.12. They reflect the effect of drop coalescences which increases as the gas density is increased, as will be discussed in Section 4.4.

The "blob" injection model has been used for a variety of spray computations including a diesel spray simulation, as shown in Fig. 3.13. The method has also been used for modeling a pressure atomized spray from a poppet nozzle by Kuo and Reitz (1992) in a study of combustion in a direct-injected two-stroke engine. In this case, the initial blob size was determined from the instantaneous liquid sheet thickness at the nozzle exit, as determined from measurements of the poppet lift. This assumption was justified by the fact that the sheet breakup length is very short under the high gas densities conditions that exist in the combustion chamber at the time of fuel injection.

There are aspects of the 'blob' breakup model that need to be addressed in future studies. The most notable assumption of the model is that the complex-shaped liquid blobs or ligaments near the nozzle can be described using only one characteristic size

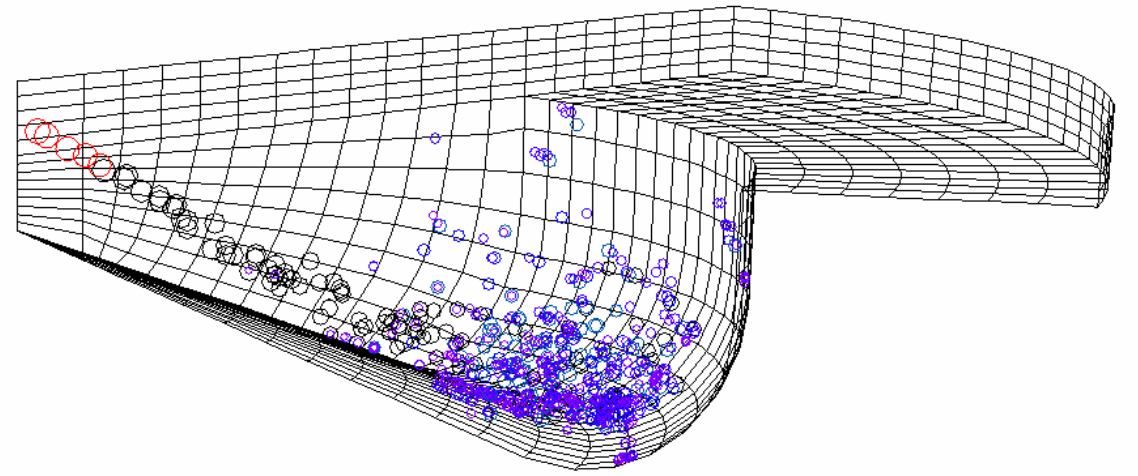

Fig. 3.13 Computational mesh showing spray parcel locations at 5 degrees after top-dead-center in a diesel engine. The spray impinges on the surface at the bottom of the piston bowl. A core region of large drops is seen near the nozzle (top left) (Patterson et al. 1994).

dimension. The model could be refined to include more detail about the shape of these ligaments, but in the absence of experimental data in the core region of high-pressure sprays, it is not clear whether this additional complexity is warranted. A second point to note is that the jet stability theory does not predict the size or the size distribution of the unstable surface waves at the moment of breakup and also the time between successive ruptures. Model constants are introduced to describe these quantities. However, the value of the constants may be influenced by events that occurred within the nozzle, or by prior breakups and collisions within the spray which would perturb the surface of the drops. The importance of these effects needs to be established by additional comparisons with experiment.